JOURNAL OF SOLID STATE CHEMISTRY 4, 123–130 (1972)

Ternary Equiatomic Transition Metal Silicides and Germanides

VANCLIFF JOHNSON AND WOLFGANG JEITSCHKO

Central Research Department, Experimental Station, E. I. du Pont de Nemours and Company, Wilmington, Delaware 19898*

Received May 27, 1971

The phases TiRhSi, TiPdSi, MnRhSi, ZrFeGe, ZrRhGe, ZrPdGe, and NbRhGe crystallize with the TiNiSi (ordered anti-$PbCl_2$) structure. ZrRuSi possesses the Fe_2P structure, while TiRuSi has the closely related TiFeSi structure. Cell parameters for these phases and a refinement of the structure of ZrRuSi from X-ray powder data are reported. Relationships among the observed structural types as well as the "filled" NiAs (Ni_2In) type are pointed out. The crystal chemistry of ternary equiatomic phases of two transition metals and silicon or germanium is discussed, emphasizing differences in metal–metal bonding.

Introduction

Many ternary phases TT'Si or TT'Ge, where T and T' are *d*-transition metals, are known (*1–7*), where T is a large, electropositive transition metal from the left side of the periodic table, e.g., Ti, Nb, while T' is a small transition metal from the iron group. For these compounds, ordered versions of the Co_2P (anti-$PbCl_2$), Fe_2P and Ni_2In, or closely related structures most frequently occur. Notable exceptions are the equiatomic silicides, where T is molybdenum or tungsten, which possess the $MgZn_2$-type structure (*2*).

The purpose of this paper is to report the existence of additional silicides and germanides with ordered anti-$PbCl_2$ (TiRhSi, TiPdSi, MnRhSi, ZrFeGe, ZrRhGe, ZrPdGe, and NbRhGe), Fe_2P (ZrRuSi), and TiFeSi (TiRuSi) structures. Metal–metal distances for representative phases with the Ni_2In, anti-$PbCl_2$, and ordered Fe_2P structures are used to discuss the crystal chemistry of these phases.

Experimental

The compounds were prepared by arc or induction melting of stoichiometric amounts of high purity (99.99%) elements. Arc melting was carried out on water-cooled copper hearths in gettered argon; high-frequency induction melting was done in vacuum or under gettered argon with Al_2O_3 (Morganite) crucibles as sample containers. Samples were annealed between 800 and 1100°C in evacuated silica or Al_2O_3-lined silica ampoules, usually followed by quick cooling. Details are given in Table I.

Powdered portions of the samples were examined by X-ray diffractometry or by the Guinier–Hägg technique (Cu$K\alpha$ radiation). Samples cooled directly from the melt and annealed samples were both studied. For cell parameter refinements, *d*-spacings were read from Guinier–Hägg photographs with a David–Mann film reader. High purity KCl ($a = 6.29310$ Å) was used for internal calibration. The lattice parameters listed in Table I were refined from the data by a computerized least-squares method. The small standard deviations listed in Table I resulted from the refinements and do not include any compositional variation of lattice constants. Calculated and observed *d* spacings agree well in all cases.

Results

Phases with TiNiSi (ordered anti-$PbCl_2$) structure. Powder patterns of TiRhSi, TiPdSi, MnRhSi, ZrFeGe, ZrRhGe, ZrPdGe, and NbRhGe were all similar and resembled that of TiNiSi (*8*). Assuming the TiNiSi positional parameters (Table II), an intensity calculation (*9*) for TiRhSi gave very good agreement between calculated and observed intensities (Table III); this confirms the TiNiSi structure.

Preparations of MnRhSi and TiPdSi persistently showed weak lines that could not be indexed on the orthorhombic cells given in Table I. On the other hand, overexposed Guinier photographs for the composition $MnRh_{0.95}Si$ prepared under similar

* Contribution No. 1811.

TABLE I

PREPARATION AND UNIT CELL DIMENSIONS OF TERNARY SILICIDES AND GERMANIDES

Composition	Type	a (Å)	b (Å)	c (Å)	V (Å^3)	Method of preparation	Heat treatment[a]
TiRuSi	TiFeSi	7.0352 ± 7	11.1920 ± 13	6.4734 ± 8	509.7	arc melting	as cast, q
TiRhSi	TiNiSi	6.2443 ± 3	3.8183 ± 3	7.2257 ± 5	172.3	arc melting	900°C, 2d, sc
TiPdSi	TiNiSi	6.3243 ± 4	3.7786 ± 7	7.3938 ± 5	176.7	arc melting	900°C, 2d, sc
ZrRuSi	Fe_2P	6.6838 ± 2		3.6717 ± 3	142.0	arc melting	as cast, q
MnRhSi	TiNiSi	6.1994 ± 4	3.7968 ± 2	7.1387 ± 3	168.0	powder sintered	1100°C, 3d, sc
$MnRh_{0.95}Si$	TiNiSi	6.1930 ± 4	3.7966 ± 3	7.1445 ± 4	168.0	induction melting	1050°C, 3d, sc
$Mn_{0.5}Pd_{1.5}Si$	Fe_2P	6.4909 ± 6		3.4655 ± 6	126.4	induction melting	950°C, 3d, q
ZrFeGe	TiNiSi	6.5185 ± 9	3.8910 ± 5	7.5425 ± 9	191.3	arc melting	840°C, 7d, q
ZrRhGe	TiNiSi	6.5923 ± 4	3.9906 ± 3	7.5620 ± 5	198.9	arc melting	840°C, 7d, q
ZrPdGe (H.T.)	TiNiSi	6.6716 ± 4	3.9536 ± 3	7.7019 ± 4	203.2	arc melting	as cast, q
NbRhGe	TiNiSi	6.4395 ± 4	3.8427 ± 3	7.4307 ± 4	183.9	arc melting	840°C, 7d, q

[a] d = days, sc = slow cooled, q = quenched.

conditions showed no extra lines. The cell volume of $MnRh_{0.95}Si$ is identical to that of "MnRhSi" so that this phase (and perhaps "TiPdSi") is homogeneous when slightly metal-deficient. This was not investigated further.

Preparations of ZrPdGe cooled directly from the melt have the TiNiSi structure, however, the major phase in samples annealed between 800 and 840°C is Fe_2P type. This indicates eutectoid decomposition of the high-temperature TiNiSi-type phase into an Fe_2P-type phase (perhaps a solid solution based on the binary Pd_2Ge) and another phase which has not been identified.

TABLE II

STRUCTURAL DATA FOR TiNiSi (ORDERED ANTI-$PbCl_2$ TYPE, E PHASE), ZrRuSi (ORDERED Fe_2P TYPE), AND TiFeSi

Atom	Position	x	y	z
	TiNiSi: space group $Pnma$-D_{2h}^{16}; $M = 4$			
Ti	4*c*	0.0212	1/4	0.1803
Ni	4*c*	0.1420	1/4	0.5609
Si	4*c*	0.7651	1/4	0.6229
	ZrRuSi: space group $P\bar{6}2m$-D_{3h}^3; $M = 3$			
Zr	3*g*	0.580 ± 0.002	0	1/2
Ru	3*f*	0.248 ± 0.002	0	0
Si	2*c*	1/3	2/3	0
Si	1*b*	0	0	1/2
	TiFeSi: space group $Ima2$-C_{2v}^{22}; $M = 12$			
Ti	4*b*	1/4	0.2004	0.2964
Ti	4*b*	1/4	0.7793	0.2707
Ti	4*b*	1/4	0.9979	0.9178
Fe	8*c*	0.0295	0.3764	0.1200
Fe	4*a*	0	0.0	0.2501
Si	8*c*	0.0060	0.1675	0.9953
Si	4*b*	1/4	0.9747	0.5055

The new phases with the TiNiSi structure have a/c and $(a + c)/b$ ratios very similar to those of other ternary transition metal borides, silicides, germanides, phosphides, and arsenides with that structure (*10*); so all belong to the Co_2P branch of the anti-$PbCl_2$ type (*11, 12*). Atomic coordinations differ substantially between the Co_2Si and Co_2P branches of the anti-$PbCl_2$ structure (*11*).

The structure of ZrRuSi. X-Ray powder patterns of ZrRuSi could be indexed with a hexagonal unit cell (Table I) based on the ordered Fe_2P-type structure. Since that structure has only two positional parameters, powder intensities were used for a least-squares refinement with 325 mesh powder, scintillation counter and Ni-filtered Cu$K\alpha$ radiation. Because the grain size was relatively large, relative intensities of some reflections with low multiplicities varied up to 50% for scans with different orientations; therefore, we averaged the intensities measured from three different scans. A least-squares program for powder intensities which accounts for overlapping peaks (*13*) was used. The calculation converged readily to the parameters given in Table II. The final R value ($R = \Sigma|I_o - I_c|/I_o$) is 0.10. When site occupancies were allowed to vary, no significant deviations from full occupancy resulted. Interatomic distances are listed in Table IV. Calculated and observed intensities are compared in Table V.

TABLE III

EVALUATION OF A GUINIER–HÄGG POWDER PATTERN OF TiRhSi WITH TiNiSi-TYPE STRUCTURE[a]

h k l	d_c	d_o	I_c	I_o	*h k l*	d_c	d_o	I_c	I_o
1 0 1	4.7246	4.7257	1000	vvs	2 2 0	1.6288	—	1	—
0 0 2	3.6129	3.6122	141	s	2 2 1	1.5889	1.5895	16	vvw
0 1 1	3.3759	3.3756	30	vw	1 1 4	1.5798	*	70	*
1 0 2	3.1271	3.1277	345	vs	3 0 3	1.5749	—	5	—
2 0 0	3.1222	—	1	—	2 0 4	1.5636	—	5	—
1 1 1	2.9697	2.9696	898	vvs	4 0 0	1.5611	—	7	—
2 0 1	2.8660	2.8654	39	w	4 0 1	1.5259	1.5260	11	vvw
1 1 2	2.4193	2.4183	588	vvs	2 2 2	1.4849	1.4850	46	m
2 1 0	2.4170		543		3 1 3	1.4559	1.4550	20	s
2 0 2	2.3623	2.3623	88	m	1 2 3	1.4550		182	
2 1 1	2.2922	2.2922	364	vs	2 1 4	1.4470	—	1	—
1 0 3	2.2472	2.2473	314	vs	4 1 0	1.4450	—	1	—
0 1 3	2.0371	2.0374	458	vs	4 0 2	1.4330	1.4331	93	m
2 1 2	2.0089	2.0089	234	s	4 1 1	1.4169	1.4169	56	w
3 0 1	2.0001	2.0004	407	vs	1 0 5	1.4079	*	60	*
1 1 3	1.9367	1.9369	83	m	3 2 1	1.3810	1.3810	302	vs
0 2 0	1.9092	1.9083	372	vvs	3 0 4	1.3643	—	5	—
2 0 3	1.9070		200		0 1 5	1.3516	1.3513	106	m
0 0 4	1.8064	—	10	—	2 2 3	1.3492	1.3494	163	s
3 0 2	1.8035	1.8037	43	w	4 1 2	1.3416	1.3416	38	w
3 1 1	1.7717	1.7713	36	m	1 1 5	1.3210	1.3207	21	vvw
1 2 1	1.7701		142		0 2 4	1.3121		9	
1 0 4	1.7353	1.7355	110	m	2 0 5	1.3115	1.3112	103	s
2 1 3	1.7061	1.7062	29	vw	3 2 2	1.3110		38	
0 2 2	1.6880	1.6882	37	w					
3 1 2	1.6308	1.6301	32	s					
1 2 2	1.6295		112						

[a] Cu$K\alpha$ radiation.
* Coincidence KCl.

$Mn_{0.5}Pd_{1.5}Si$ and TiRuSi. Preparations of MnPdSi were not single phase. The X-ray powder pattern contained lines which indicated the presence of an Fe_2P-type structure. We believe this phase is a member of a solid solution series based on Pd_2Si and not a true ternary phase. Consistent with this belief, $Mn_{0.5}Pd_{1.5}Si$ was single phase at 950°C whereas at 750°C the solubility does not extend to this composition. The lattice constants for this composition, quenched from 950°C, are given in Table I.

TABLE IV

INTERATOMIC DISTANCES (Å) IN THE STRUCTURE OF ZrRuSi[a]

Zr:	4 Zr 3.467	Ru:	2 Zr 2.879
	2 Ru 2.879		4 Zr 3.056
	4 Ru 3.056		2 Ru 2.871
	4 Si 2.716		2 Si 2.561
	1 Si 2.807		2 Si 2.473
Si(2c):	6 Zr 2.716	Si(1b):	3 Zr 2.807
	3 Ru 2.561		6 Ru 2.473

[a] Standard deviations are all less than 0.01 Å. All distances shorter than 3.8 Å are listed.

The Guinier–Hägg powder pattern of TiRuSi closely resembled that of ZrRuSi. However, some lines were broadened or split, and there were additional weak lines which could not be indexed with an Fe_2P-type cell. This has also been observed for TiFeSi which has a superstructure (*6*) based on the Fe_2P type with orthorhombic distortion, resulting in a quadrupling of the unit cell volume. Indeed, the additional weak lines could be indexed with a TiFeSi-type unit cell (Table II) and an intensity calculation (*9*) using TiFeSi positional parameters further confirmed this structure for TiRuSi (Table VI).

TABLE V

CALCULATED AND OBSERVED INTENSITIES FOR ZrRuSi WITH ORDERED Fe_2P-TYPE STRUCTURE[a]

$h\,k\,l$	d_c	d_o	I_c	I_o	$h\,k\,l$	d_c	d_o	I_c	I_o
1 0 0	5.7883	5.7788	41	36	4 0 0	1.4471	1.4472	50	48
0 0 1	3.6717	3.6696	15	11	2 1 2	1.4063	1.4065	224	212
1 1 0	3.3419	3.3405	140	128	4 0 1	1.3463	1.3462	38	36
1 0 1	3.1005	3.0995	183	171	3 0 2	1.3300	1.3299	46	72
2 0 0	2.8942	2.8934	43	35	3 2 0	1.3279	1.3280	17	
1 1 1	2.4715	2.4715	948	1000	4 1 0	1.2631	1.2630	16	13
2 0 1	2.2730	2.2731	649	769	3 2 1	1.2488	1.2487	139	106
2 1 0	2.1878	2.1880	608	603	2 2 2	1.2357	*	4	8
3 0 0	1.9294	1.9294	100	93	0 0 3	1.2239	*	0	1
2 1 1	1.8794	1.8794	119	142	3 1 2	1.2085	*	44	57
0 0 2	1.8359	1.8361	186	162	1 0 3	1.1974	*	6	55
1 0 2	1.7499	—	2	1	4 1 1	1.1944	*	38	
3 0 1	1.7080	—	4	3	5 0 0	1.1577	*	24	29
2 2 0	1.6710	1.6710	7	7	1 1 3	1.1493	*	51	72
1 1 2	1.6090	1.6090	26	103	4 0 2	1.1365	*	37	55
3 1 0	1.6054	1.6055	71		2 0 3	1.1272	*	43	43
2 0 2	1.5503	1.5502	11	8	3 3 0	1.1140	*	31	23
2 2 1	1.5209	1.5211	26	25	5 0 1	1.1041	*	11	8
3 1 1	1.4709	1.4711	165	149	4 2 0	1.0939	*	16	21

[a] Intensities were obtained from powder diffractometer scans, d-spacings (Å) from a Guinier–Hägg camera. Cu$K\alpha$ radiation.
* Data not on Guinier–Hägg film.

The TiFeSi structure can be derived from the ordered Fe_2P-type structure through small distortions (*6*). No interchange of atoms is involved. Similar structural relations are known between the low- and high-temperature phases of quartz, VO_2, $BaTiO_3$, and others. One might expect TiRuSi to transform diffusionlessly on heating to the ordered Fe_2P-type structure. However, a sensitive DSC analysis on TiRuSi did not show any obvious transitions up to 1000°C.

Discussion

The new ternary transition metal silicides and germanides are listed in Table VII along with phases from other sources (*1–8*, *14*). The TiNiSi structure occurs most frequently. The Fe_2P- and the closely related TiFeSi-type phases have lower overall electron concentrations. They are most frequently found with the rare earth metals as T component and with elements from the aluminum group replacing silicon or germanium (*15*). The table also shows relatively confined regions for the $MgZn_2$ and Ni_2In-type structures. The $MgZn_2$-type structure has characteristics typical of intermetallic compounds and will not be discussed further. All other structures are closely related.

The Ni_2In structure has generally been regarded as a "filled up" version of the NiAs structure. In the NiAs structure, the metalloid atoms (As) form a hexagonal, close-packed array with octahedral and trigonal bi-pyramidal voids. Only octahedral voids are occupied in NiAs, whereas both are in Ni_2In. MnP and TiNiSi are similarly related. The MnP structure derives from the NiAs structure by small atomic displacements; likewise, the TiNiSi structure may be regarded as a distorted Ni_2In structure (*16*). These structural relationships are shown in Fig. 1. The basic triangular prismatic coordination of the metalloid atom in NiAs is retained in all these structures, suggesting similar metal–metalloid bonding (*17*).

Phases with the NiAs structure and low c/a ratios have short metal–metal distances along the c axis. The transition metal d orbitals of t_{2g} symmetry are split into two $t_\perp$ and one $t_\parallel$ orbital per metal atom by the hexagonal symmetry; the $t_\parallel$ orbitals of neighboring cations overlap to form bands and contribute to the binding energy. Since for highly positive cations short metal–metal distances introduce core electrostatic repulsions, structures with short metal–metal distances are usually not adopted by ionic compounds. However, in compounds of transition metals with the less electronegative

TABLE VI

CALCULATED AND OBSERVED *d*-SPACINGS (Å) AND INTENSITIES FOR TiRuSi WITH TiFeSi-TYPE STRUCTURE[a]

*h k l**	*h k l*	d_c	d_o	I_c	I_o	*h k l**	*h k l*	d_c	d_o	I_c	I_o
	1 1 0	5.9562	5.9500	31	vw	1 0 2	4 1 1	1.6781	—	12	—
1 0 0	0 1 1	5.6036	5.5981	281	vs		4 2 0	1.6779	—	11	—
	0 2 0	5.5960		132			1 4 3	1.6604	—	0	—
	1 2 1	3.6274	3.6245	32	vw	3 0 1	2 3 3	1.6497	1.6491	25	w
0 0 1	2 0 0	3.5176	3.5168	305	vs		2 6 0	1.6480		18	
	1 3 0	3.2959	—	10	—		3 5 0	1.6192	—	2	—
1 1 0	0 0 2	3.2367	3.2323	148	vs	2 2 0	0 0 4	1.6184	—	3	—
	0 3 1	3.2323		285			0 6 2	1.6162	—	6	—
1 0 1	2 1 1	2.9793	2.9783	153	s		1 1 4	1.5617	1.5608	10	vvw
	2 2 0	2.9781		87			1 7 0	1.5591	—	1	—
	1 1 2	2.8439	—	5	—		0 2 4	1.5547		13	
2 0 0	0 2 2	2.8018	—	0	—	3 1 0	0 5 3	1.5535	1.5535	18	w
	0 4 0	2.7980	—	1	—		0 7 1	1.5522		15	
	1 4 1	2.4126	—	7	—	1 1 2	4 0 2	1.5454	1.5451	17	w
1 1 1	2 0 2	2.3818	2.3809	447	vvs		4 3 1	1.5449		37	
	2 3 1	2.3801		1000			3 2 3	1.5276	1.5281	31	vw
	1 3 2	2.3094	2.3086	22	vw	2 0 2	4 2 2	1.4896	—	0	—
	3 1 0	2.2952	2.2958	45	w		4 4 0	1.4891	—	2	—
2 0 1	2 2 2	2.1916	2.1914	653	vvs	2 2 1	2 0 4	1.4702	1.4687	12	w
	2 4 0	2.1897		274			2 6 2	1.4688		26	
	1 5 0	2.1330	2.1330	28	vw		1 3 4	1.4527	—	1	
	0 1 3	2.1188		419			3 5 2	1.4481	1.4480	17	w
2 1 0	0 4 2	2.1167	2.1173	392	vvs		3 6 1	1.4241	1.4237	23	vw
	0 5 1	2.1155		402			2 2 4	1.4220		53	
	3 2 1	2.0514	2.0517	105	m	3 1 1	2 5 3	1.4211	1.4214	49	s
	3 3 0	1.9854	1.9853	24	vw		2 7 1	1.4201		60	
	1 2 3	1.9356	1.9360	22	vw		1 7 2	1.4046	—	13	
	3 1 2	1.8723	1.8719	48	w	4 0 0	0 4 4	1.4009	1.4008	117	m
3 0 0	0 3 3	1.8679	1.8680	131	s		0 8 0	1.3990	1.3991	52	w
	0 6 0	1.8653		62			5 1 0	1.3961	—	16	—
	2 1 3	1.8150		206			1 6 3	1.3836	—	5	—
2 1 1	2 4 2	1.8137	1.8144	213	vvs		3 4 3	1.3810	—	0	
	2 5 1	1.8129		204			4 1 3	1.3533		145	
	1 5 2	1.7811	—	2	—	2 1 2	4 4 2	1.3528	1.3528	123	vs
0 0 2	4 0 0	1.7588	1.7591	282	vs		4 5 1	1.3524		138	
	1 6 1	1.7369	—	12	—		1 8 1	1.3423	—	3	—
	3 4 1	1.7318	—	5	—		5 2 1	1.3352	1.3350	44	w
	3 3 2	1.6924	1.6932	28	vw						

[a] Guinier–Hägg camera, Cu$K\alpha$ radiation.
* Indices of Fe_2P-like subcell.

nonmetals (metalloids of groups IVB and VB), the effective charges on the metal atoms are small, and metal–metal bonding more than compensates for the electrostatic repulsions introduced by short metal–metal distances. These ideas have been suggested by Goodenough (*18*) who discussed the crystal chemistry of binary pnictides and chalcogenides with NiAs-related structures. The influence of metal–metal bonding and its increased importance in the highly covalent metalloid phases are illustrated by the following empirical findings (*19*):

(1) NiAs phases do not occur among the more ionic oxides and halides, nor with nontransition metals that are not capable of *d*-electron metal–metal bonding.

(2) The MnP structure, with an even greater number of short metal–metal distances than the NiAs structure, occurs when the metalloid is of groups IVB and VB but seldom when it is the more electronegative chalcogen.

(3) There is a tendency to form "metal-filled" NiAs-related structures with more and shorter

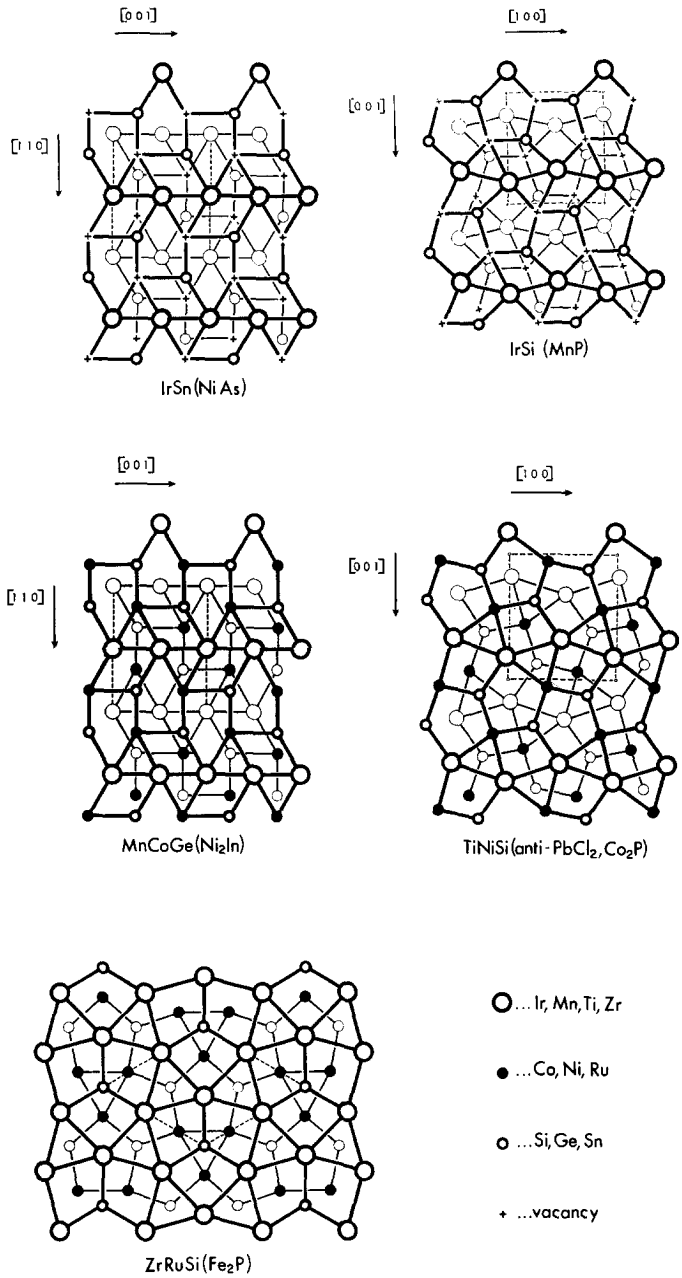

FIG. 1. Projections of the structures of IrSn, IrSi, MnCoGe, TiNiSi, and ZrRuSi. The respective structure types are given in parentheses. Atoms connected by thick and thin lines are separated by half a translation period in the projection direction. Atoms and vacancies are connected to emphasize relationships and differences among the structures.

metal–metal distances as the metalloid component becomes less electronegative.

Since bonding between transition metals and silicon or germanium is essentially covalent, metal–metal bonding apparently contributes enough to the binding energy so that "metal-filled", NiAs-related structures are frequently found for phases with these elements. Since the basic metalloid environment is retained in the several variants of the "filled" NiAs structure, one might ask how metal–metal bonding influences the particular structural choice.

Structures of a few silicides with various "filled", NiAs-related structures have been refined. The

TABLE VII

OCCURRENCE OF TERNARY EQUIATOMIC TRANSITION METAL SILICIDES AND GERMANIDES TT'Si(Ge)

	SILICIDES					GERMANIDES				
T = \ T' =	Mn	Fe	Co	Ni	Cu	Mn	Fe	Co	Ni	Cu
Ti	○	●	□	□	□		●	○	□	□
Zr		□	□	□	□		□	□	□	□
Hf		□	□	□	□		○	□	□	□
V			□	□				□	□	
Nb	○	□	□	□		○	●	□	□	
Ta		□	□	□			□	□	□	
Cr										
Mo		×	×	×						
W		×	×	×						
Mn			□	□			△	△	△	
	Tc	Ru	Rh	Pd	Ag	Tc	Ru	Rh	Pd	Ag
Ti		●	□	□						
Zr		○		□			●	□	□	
Nb								□		
Mn			□							

□.....TiNiSi (anti-$PbCl_2$)
○.....Fe_2P
●.....TiFeSi
×.....$MgZn_2$
△.....Ni_2In

metal–metal distances for one example of each are given in Table VIII (the TiFeSi type has not been included since, for our purpose, its distortion from the Fe_2P type is insignificant). The structures of TiNiSi and ZrRuSi differ from the MnCoGe structure in the respective T–T distances. In MnCoGe, these distances are shorter. Apparently, the more electropositive Ti and Zr are more highly charged than Mn in these compounds. It is therefore understandable that the T–T distances in TiNiSi and ZrRuSi are longer than in MnCoGe. Thus, TiNiSi and ZrRuSi do not adopt the Ni_2In structure because the T atoms would approach too closely.

In TiNiSi and ZrRuSi, the T'–T' distances are, however, much shorter than in MnCoGe. There is therefore a larger number of metal–metal bonds in the TiNiSi and ordered Fe_2P types than in the ordered Ni_2In-type structure. The seeming unimportance of the T'–T' interactions to the stability of the Ni_2In structure may well account for the frequent occurrence of this structure for phases with extended homogeneity ranges arising from variability in the T' concentration. Conversely, phases with the anti-$PbCl_2$ and Fe_2P structures usually exist over more restricted homogeneity ranges.

The atomic environments in the TiNiSi and ordered Fe_2P-type silicides and germanides are very similar (*6*). Interatomic distances showed no systematic trends. Since the ordered Fe_2P-type phases occur most frequently with the rare earth elements as T component and aluminum as "metalloid," the lower valence electron concentration of the Fe_2P silicides and germanides is probably important.

Acknowledgments

Thanks are due to J. A. Amalfitano and D. M. Graham for competent help in preparing samples and drawing figures. The authors also wish to acknowledge the help of Miss M. S. Licis with the X-ray work.

References

1. W. JEITSCHKO, A. G. JORDAN, AND P. A. BECK, *Trans. Met. Soc. AIME* **245**, 335 (1969).
2. E. I. GLADYSHEVSKII AND YU. B. KUZ'MA, *J. Struct. Chem. USSR* **1**, 57 (1960).
3. E. GANGLBERGER, H. NOWOTNY, AND F. BENESOVSKY, *Monatsh. Chem.* **98**, 95 (1967).
4. J. NICKL AND H. SPRENGER, *Naturwissenschaften* **54**, 248 and 515 (1967).
5. B. DEYRIS, J. ROY-MONTREUIL, R. FRUCHART, AND A. MICHEL, *Bull. Soc. Chim. Fr.* **1968**, 1303 (1968).

TABLE VIII

DISTANCES BETWEEN THE TRANSITION METAL ATOMS IN TERNARY SILICIDES AND GERMANIDES TT'Si(Ge)[a]

Phase	Structure type	T–T	$2r_T$	T'–T'	$2r_{T'}$	T–T'	$r_T + r_{T'}$	Reference
MnCoGe	ordered Ni_2In	2.63(2*x*) 4.04(6*x*)	2.62	3.51(6*x*)	2.52	2.68(6*x*)	2.57	(*14*)
TiNiSi	ordered anti-$PbCl_2$	3.14(2*x*) 3.23(2*x*)	2.92	2.67(2*x*)	2.48	2.77(3*x*) 2.88(3*x*)	2.70	(*8*)
ZrRuSi	ordered Fe_2P	3.47(4*x*)	3.20	2.87(2*x*)	2.64	2.88(2*x*) 3.06(4*x*)	2.78	This work

[a] The distances (Å) are compared with the sum of the atomic radii for coordination number 12.

6. W. JEITSCHKO, *Acta Crystallogr. B* **26**, 815 (1970).
7. W. JEITSCHKO, *Met. Trans.* **1**, 2963 (1970).
8. C. B. SHOEMAKER AND D. P. SHOEMAKER, *Acta Crystallogr.* **18**, 900 (1965).
9. K. YVON, W. JEITSCHKO, AND E. PARTHÉ, "A Fortran IV Program for the Intensity Calculation of Powder Patterns," Report of the Laboratory for Research on the Structure of Matter, University of Pennsylvania, Philadelphia, PA, 1969.
10. W. JEITSCHKO, *Acta Crystallogr. B* **24**, 930 (1968).
11. S. RUNDQVIST, *Arkiv Kemi.* **20**, 67 (1960).
12. S. RUNDQVIST AND P. C. NAWAPONG, *Acta Chem. Scand.* **20**, 2250 (1966).
13. C. T. PREWITT, unpublished computer program for the least-squares refinement of crystal structures.
14. L. CASTELLIZ, *Monatsh. Chem.* **84**, 765 (1953).
15. A. E. DWIGHT, M. H. MUELLER, R. A. CONNER, JR., J. W. DOWNEY, AND H. KNOTT, *Trans. Met. Soc. AIME* **242**, 2075 (1968).
16. F. JELLINEK, *Z. Osterr. Chem.* **60**, 311 (1959).
17. R. FRUCHART, A. ROGER, AND J. P. SENATEUR, *J. Appl. Phys.* **40**, 1250 (1969).
18. J. B. GOODENOUGH, Lincoln Laboratory Technical Report 345, pp. 11–12, 1964.
19. A. KJEKSHUS AND W. B. PEARSON, *Progr. Solid State Chem.* **1**, 89 (1964).